Nonlinear Dyn (2021) 104:3975–3990
https://doi.org/10.1007/s11071-021-06481-5

ORIGINAL PAPER

Parameter identification of nonlinear structural systems through frequency response sensitivity analysis

Wenlong Li · Yanmao Chen · Zhong-Rong Lu · Jike Liu · Li Wang

Received: 9 December 2020 / Accepted: 17 April 2021 / Published online: 29 April 2021

Abstract Nonlinearity is ubiquitously encountered in structural systems, and it may have a great and complicated influence on the dynamic behaviours, including bifurcation, internal resonance, load history dependence, etc. Identifying the nonlinear system parameters is essential for analysis and design of the structure. To this end, a new approach is developed in this paper for nonlinear system parameter identification from frequency response sensitivity analysis. At first, the harmonic balance equation is established to govern the frequency response of the nonlinear system, upon which the frequency response and sensitivity analysis can be conducted. A remarkable feature is that the harmonic balance equation is algebraic so that the sensitivity analysis, pertaining to a linearized equation, is rather simple and straightforward. Then, parameter identification is modelled as a nonlinear least-squares problem, and the sensitivity approach is adopted in conjunction with the trust-region constraint for convergent solution. Numerical examples are conducted to demonstrate the feasibility and performance of the proposed approach.

Keywords Parameter identification · Nonlinear structural system · Harmonic balance method · Frequency response sensitivity analysis · Trust-region constraint

W. Li · Y. Chen · Z.-R. Lu · J. Liu · L. Wang (✉)
Department of Applied Mechanics and Engineering, Sun Yat-sen University, Guangzhou 510006, People's Republic of China
e-mail: wangli75@mail.sysu.edu.cn

1 Introduction

Parameter identification of nonlinear structural systems has attracted tremendous interests from various engineering fields [1–4]. To mention a few, identification of the nonlinear aeroelastic parameters is central to design of the airfoil-store system [3]; breathing cracks [4] and plastic damages [5] are typical nonlinear damage patterns in structures and identifying these nonlinear damages constitutes one main part of structural health monitoring; for bolt jointed structures, calibration of the nonlinear bolted joint models [6] is a premise for analysis and design of the structures. The dynamic behaviours of the nonlinear systems such as bifurcation, internal resonance, and load history dependence [7] depend critically on the system parameters [8,9], and as a result, it is of great significance to identify the parameters either directly by specialized measurement instruments or inversely from response data. Generally, direct calibration of some parameters by instruments is difficult and even unavailable, and therefore, in this paper, the focus is on inverse identification of nonlinear system parameters from measured response data.

In general, parameter identification using measured response data belongs to the class of inverse problem and such problem can be formulated as a nonlinear optimization problem of which the objective function is just least squares of the residuals between the calculated response data from system equations and the measured response data. As a common way to solve the

optimization problem, meta-heuristic algorithms such as genetic algorithm [10,11], particle swarm algorithm [12], artificial bee colony algorithm [13,14] have been widely used in system parameter identification. Meta-heuristic algorithms have the strong ability to search the globally optimal solution whereas admit a quite slow convergence because of the inherent random attribute, leading to prohibitive computation cost.

In contrast to the meta-heuristic algorithms, gradient-based methods [15] only require a few iterations, and therefore, take much less computation time. To solve the optimization problem of parameter identification, the Newton method is often applied. However, when applying the Newton method, the Hessian matrix shall be obtained by the second-order sensitivity analysis, which is rather complex and computationally expensive. In addition to the Newton method, the sensitivity approach [16] only involves the first-order sensitivity analysis, tending to be simpler and more applicable. Recently, the sensitivity approach was enhanced by additionally considering the trust-region constraint so that guaranteed convergence is achieved [17]. The enhanced sensitivity approach has been successfully applied to a number of inverse problems [18–20] and therefore, is further followed up in this paper.

Regarding the data used for inverse parameter identification, the frequency response data are preferred in this paper. The reasons are mainly twofold. On the one hand, it is not always easy to determine the complete initial conditions of a dynamic structural system. Such initial conditions have a crucial influence on the time response data, while they are generally not involved in the frequency response data because the frequency response is obtained at the steady state of the structure. On the other hand, distinct to the ordinary differential equation that governs the time response data, the frequency response data pertain to the harmonic balance equation which is an algebraic equation. As a result, sensitivity analysis of the algebraic harmonic balance equation, by solving a linearized equation, is rather simple and straightforward. Though having the above two advantages, the frequency response data are mainly used for linear system parameter identification [21,22], while the application to nonlinear system identification is rather limited. Peng et al. [23,24] extended the frequency response function in linear systems to nonlinear systems by resorting to the Volterra series and then identified the system parameters from the nonlinear output frequency response function. However, the Volterra series description of frequency response is hardly available for non-smooth systems, which restricts the applications. In this paper, the harmonic balance equation is called to govern the frequency response of the nonlinear structural system due to its sound applicability to large-scale, smooth/non-smooth systems [25].

The rest of this paper is structured as follows. In Sect. 2, the harmonic balance equation is established to govern the frequency response of nonlinear structural systems. Then, in Sect. 3, the sensitivity approach is developed for general nonlinear system parameter identification. In doing so, the frequency response sensitivity analysis is conducted to get the sensitivity matrix, while the trust-region constraint is introduced to enhance the convergence of the approach. In Sect. 4, numerical examples are conducted to verify the performance of the proposed approach and final conclusions are drawn in Sect. 5.

2 Harmonic balance for nonlinear structural vibration

The general form of the governing equation for dynamic motion of a m-DOF nonlinear structural system is given as follows:

$$\mathbf{M}\ddot{\boldsymbol{u}} + \mathbf{C}\dot{\boldsymbol{u}} + \mathbf{K}\boldsymbol{u} + \boldsymbol{f}_{nl}(\dot{\boldsymbol{u}}, \boldsymbol{u}) = \boldsymbol{f}(t) \tag{1}$$

where $\mathbf{M}$, $\mathbf{C}$, $\mathbf{K}$ are respective mass, damping and stiffness matrices, $\boldsymbol{u}, \dot{\boldsymbol{u}}, \ddot{\boldsymbol{u}}$ are displacement, velocity and acceleration vectors, $\boldsymbol{f}_{nl}(\dot{\boldsymbol{u}}, \boldsymbol{u})$ and $\boldsymbol{f}(t)$ denote the nonlinear restoring forces and the external forces. The parameters to be identified of the nonlinear system are denoted by $\boldsymbol{p} = (p_1, p_2, \ldots, p_n) \in \mathcal{A}$ with $\mathcal{A}$ the feasible parametric space and may contain those in $\mathbf{M}$, $\mathbf{C}$, $\mathbf{K}$ and $\boldsymbol{f}_{nl}(\dot{\boldsymbol{u}}, \boldsymbol{u})$.

The frequency response of a nonlinear system shall be viewed as the steady-state solution under the harmonic external forces. To compute the frequency response, the external forces are set to be harmonic, e.g. $\boldsymbol{f}(t) = \boldsymbol{f}_0 \cos(\omega t)$ with $\boldsymbol{f}_0$ denoting the force amplitude vector so that the steady-state solution is generally periodic. The harmonic balance method (HBM) [25] is a celebrated method to get the periodic solution, and it uses the truncated Fourier series to represent the displacement:

$$\boldsymbol{u} = \boldsymbol{a}_0 + \sum_{n=1}^{N} [\boldsymbol{a}_n \cos(n\omega t) + \boldsymbol{b}_n \sin(n\omega t)] \tag{2}$$

where $\boldsymbol{a}_n$ and $\boldsymbol{b}_n$ are, respectively, the nth coefficient vector of the cosine and sine harmonic terms, and N denotes the order of the truncated Fourier series, or harmonic order.

According to Eq. (2), the Fourier series of the velocity and acceleration are

$$\dot{\boldsymbol{u}} = \sum_{n=1}^{N} n\omega \left[\boldsymbol{b}_n \cos(n\omega t) - \boldsymbol{a}_n \sin(n\omega t)\right] \tag{3}$$

$$\ddot{\boldsymbol{u}} = \sum_{n=1}^{N} -(n\omega)^2 \left[\boldsymbol{a}_n \cos(n\omega t) + \boldsymbol{b}_n \sin(n\omega t)\right] \tag{4}$$

Then, the HBM, as a Galerkin-type method, establishes the following equations for the coefficients:

$$\begin{cases} \frac{1}{T}\int_0^{\mathrm{T}} [\mathbf{M}\ddot{\boldsymbol{u}} + \mathbf{C}\dot{\boldsymbol{u}} + \mathbf{K}\boldsymbol{u} + \boldsymbol{f}_{nl}(\dot{\boldsymbol{u}}, \boldsymbol{u}) - \boldsymbol{f}(t)]\mathrm{d}t = \mathbf{0} \\ \frac{2}{T}\int_0^{\mathrm{T}} \cos(\omega t)[\mathbf{M}\ddot{\boldsymbol{u}} + \mathbf{C}\dot{\boldsymbol{u}} + \mathbf{K}\boldsymbol{u} + \boldsymbol{f}_{nl}(\dot{\boldsymbol{u}}, \boldsymbol{u}) - \boldsymbol{f}(t)]\mathrm{d}t = \mathbf{0} \\ \frac{2}{T}\int_0^{\mathrm{T}} \sin(\omega t)[\mathbf{M}\ddot{\boldsymbol{u}} + \mathbf{C}\dot{\boldsymbol{u}} + \mathbf{K}\boldsymbol{u} + \boldsymbol{f}_{nl}(\dot{\boldsymbol{u}}, \boldsymbol{u}) - \boldsymbol{f}(t)]\mathrm{d}t = \mathbf{0} \\ \vdots \\ \frac{2}{T}\int_0^{\mathrm{T}} \cos(N\omega t)[\mathbf{M}\ddot{\boldsymbol{u}} + \mathbf{C}\dot{\boldsymbol{u}} + \mathbf{K}\boldsymbol{u} + \boldsymbol{f}_{nl}(\dot{\boldsymbol{u}}, \boldsymbol{u}) - \boldsymbol{f}(t)]\mathrm{d}t = \mathbf{0} \\ \frac{2}{T}\int_0^{\mathrm{T}} \sin(N\omega t)[\mathbf{M}\ddot{\boldsymbol{u}} + \mathbf{C}\dot{\boldsymbol{u}} + \mathbf{K}\boldsymbol{u} + \boldsymbol{f}_{nl}(\dot{\boldsymbol{u}}, \boldsymbol{u}) - \boldsymbol{f}(t)]\mathrm{d}t = \mathbf{0} \end{cases} \tag{5}$$

where $T = \frac{2\pi}{\omega}$. The above equation can also be regrouped in a more concise form [25]:

$$\mathbf{A}(\omega)\boldsymbol{z} + \boldsymbol{F}_{nl}(\omega, \boldsymbol{z}) = \boldsymbol{F} \tag{6}$$

where

- $\boldsymbol{z} = [\boldsymbol{a}_0; \boldsymbol{a}_1; \boldsymbol{b}_1; \ldots; \boldsymbol{a}_N, \boldsymbol{b}_N]$ collect all coefficients in a column vector,

$$\mathbf{A}(\omega) = \begin{bmatrix} \mathbf{K} & & & & \\ & \mathbf{K}-\omega^2\mathbf{M} & \omega\mathbf{C} & & \\ & -\omega\mathbf{C} & \mathbf{K}-\omega^2\mathbf{M} & & \\ & & & \ddots & \\ & & & \mathbf{K}-(N\omega)^2\mathbf{M} & N\omega\mathbf{C} \\ & & & -N\omega\mathbf{C} & \mathbf{K}-(N\omega)^2\mathbf{M} \end{bmatrix}, \tag{7}$$

- $$\begin{aligned} &\boldsymbol{F}_{nl}(\omega, \boldsymbol{z}) \\ &= \Bigg[\frac{1}{T}\int_0^{\mathrm{T}} \boldsymbol{f}_{nl}(\dot{\boldsymbol{u}}, \boldsymbol{u})\mathrm{d}t; \\ &\quad \frac{2}{T}\int_0^{\mathrm{T}} \cos(\omega t)\boldsymbol{f}_{nl}(\dot{\boldsymbol{u}}, \boldsymbol{u})\mathrm{d}t; \\ &\quad \frac{2}{T}\int_0^{\mathrm{T}} \sin(\omega t)\boldsymbol{f}_{nl}(\dot{\boldsymbol{u}}, \boldsymbol{u})\mathrm{d}t; \\ &\quad \ldots; \frac{2}{T}\int_0^{\mathrm{T}} \cos(N\omega t)\boldsymbol{f}_{nl}(\dot{\boldsymbol{u}}, \boldsymbol{u})\mathrm{d}t; \\ &\quad \frac{2}{T}\int_0^{\mathrm{T}} \sin(N\omega t)\boldsymbol{f}_{nl}(\dot{\boldsymbol{u}}, \boldsymbol{u})\mathrm{d}t\Bigg] \end{aligned}$$

  denote the Fourier coefficients of the nonlinear restoring forces $\boldsymbol{f}_{nl}(\dot{\boldsymbol{u}}, \boldsymbol{u})$ and can be quickly computed by resorting to the alternating frequency-time (AFT) scheme [25,26].
- $\boldsymbol{F}$ are the Fourier coefficients of the external forces $\boldsymbol{f}(t)$, and herein, they are of the form: $\boldsymbol{F} = [\mathbf{0}; \boldsymbol{f}_0; \mathbf{0}; \ldots; \mathbf{0}; \mathbf{0}]$.

$\boldsymbol{z}$ is also called the (generalized) frequency response of the nonlinear system and Eq. (6), termed the *harmonic balance equation*, turns out to govern the nonlinear frequency response $\boldsymbol{z}$. The Newton–Raphson method is often used to get the solution of the nonlinear algebraic equation. Note that the solution may be non-unique at some frequency and it depends on the initial conditions (or load history). In this paper, the frequency response under a number of frequencies is considered for iterative parameter identification and the following strategy is adopted to solve Eq. (6):

- At the first iteration, numerical continuation is used where the calculation can proceed firstly for a frequency with simply unique solution and then continue numerically for other frequencies by selecting the already obtained solution of a nearby frequency as initial guess. This corresponds to the calculation of the response under $\boldsymbol{p}^{(0)}$ in Algorithm 1.
- In subsequent iterations, the frequency response at a certain frequency is then computed by setting the corresponding solution in the previous iteration as initial guess. In Algorithm 1, these are used in the calculation of the response under $\boldsymbol{p}^{(k)}, k \geq 1$ and $\boldsymbol{p}^{(k)} + \Delta\boldsymbol{p}, k \geq 0$.

It is also noteworthy that $\boldsymbol{z}$ depends on the frequency ω, the amplitude $\boldsymbol{f}_0$ and the parameters $\boldsymbol{p}$ and therefore, it is set $\boldsymbol{z} = \boldsymbol{z}(\omega, \boldsymbol{f}_0, \boldsymbol{p})$. As with the selection of harmonic order N, it depends on the smoothness of the systems: N is usually small (e.g. $N = 3$) for smooth systems, while for non-smooth systems, greater N is required. For parameter identification, part of the response data are measured and one can directly determine N so that higher-order (greater than N) harmonics of the data are negligible.

3 Parameter identification by nonlinear frequency response sensitivity analysis

3.1 Inverse formulation of parameter identification

Assume that a number of harmonic loads with different frequencies ω_i or amplitudes $\boldsymbol{f}_i$, represented by $(\omega_i, \boldsymbol{f}_i), i = 1, 2, \ldots, l$, are independently enforced on the nonlinear structure. As a consequence, given the parameters $\boldsymbol{p}$, the frequency responses are respective $z(\omega_i, \boldsymbol{f}_i, \boldsymbol{p}), i = 1, 2, \ldots, l$. For the measured frequency response quantity $\boldsymbol{d}$, it is often incomplete and linearly dependent on the total frequency response z, i.e.

$$\boldsymbol{d} = \mathbf{L}z \tag{8}$$

where $\mathbf{L}$ is a selection matrix with full row rank. For instance, if only the basic (first-order) frequency responses $\boldsymbol{a}_1, \boldsymbol{b}_1$ are measured, there is

$$\mathbf{L} = \begin{bmatrix} \mathbf{0} & \mathbf{I} & \mathbf{0} & \mathbf{0} & \cdots & \mathbf{0} \\ \mathbf{0} & \mathbf{0} & \mathbf{I} & \mathbf{0} & \cdots & \mathbf{0} \end{bmatrix} \tag{9}$$

where $\mathbf{0}$ and $\mathbf{I}$ are respectively zero and identity matrices, both of order m. Under different harmonic loads $(\omega_i, \boldsymbol{f}_i)$, the measured frequency response data are denoted by $\hat{\boldsymbol{d}}(\omega_i, \boldsymbol{f}_i)$ and are collected in a column vector:

$$\hat{\boldsymbol{R}} = \begin{bmatrix} \hat{\boldsymbol{d}}(\omega_1, \boldsymbol{f}_1) \\ \hat{\boldsymbol{d}}(\omega_2, \boldsymbol{f}_2) \\ \vdots \\ \hat{\boldsymbol{d}}(\omega_l, \boldsymbol{f}_l) \end{bmatrix}. \tag{10}$$

In correspondence to the measured data, the calculated data from the governing equation are denoted by $\boldsymbol{d}(\omega_i, \boldsymbol{f}_i, \boldsymbol{p}) = \mathbf{L}z(\omega_i, \boldsymbol{f}_i, \boldsymbol{p})$ and are also collected in a column vector

$$\boldsymbol{R}(\boldsymbol{p}) = \begin{bmatrix} \boldsymbol{d}(\omega_1, \boldsymbol{f}_1, \boldsymbol{p}) \\ \boldsymbol{d}(\omega_2, \boldsymbol{f}_2, \boldsymbol{p}) \\ \vdots \\ \boldsymbol{d}(\omega_l, \boldsymbol{f}_l, \boldsymbol{p}) \end{bmatrix} = \begin{bmatrix} \mathbf{L}z(\omega_1, \boldsymbol{f}_1, \boldsymbol{p}) \\ \mathbf{L}z(\omega_2, \boldsymbol{f}_2, \boldsymbol{p}) \\ \vdots \\ \mathbf{L}z(\omega_l, \boldsymbol{f}_l, \boldsymbol{p}) \end{bmatrix}. \tag{11}$$

Then, following the general idea of inverse problem, parameter identification is formulated as: find the parameters $\boldsymbol{p}$ such that the least squares of the misfit between the measured and calculated data is minimized, leading to the following nonlinear optimization problem:

$$\boldsymbol{p}^* = \arg\min_{\boldsymbol{p}\in\mathcal{A}} \left\{ g(\boldsymbol{p}) := \|\hat{\boldsymbol{R}} - \boldsymbol{R}(\boldsymbol{p})\|_{\mathbf{W}}^2 \right\} \tag{12}$$

where $g(\boldsymbol{p})$ is the goal function, $\|(\cdot)\|_{\mathbf{W}} = \sqrt{(\cdot)\mathbf{W}(\cdot)}$, and $\mathbf{W}$ denotes the user-defined positive define (and often diagonal) weight matrix which is usually set inverse proportional to the covariance of measurement errors [27].

As is noteworthy, bifurcations may arise for a nonlinear system. Under this circumstance, to still identify with the goal function (12), some special treatments should be invoked. Herein, two main cases are addressed in the presence of bifurcations:

- On the one hand, the periodic solution may be non-unique, depending on whether the excitation frequency is sweeping decreasingly or increasingly. For this case, to get reasonable identification, numerical continuation of the solution should be consistent with the sweeping frequency. For instance, if the excitation frequency is sweeping increasingly (resp. decreasingly), the continuation shall also be performed along the lines of increasing (resp. decreasing) frequency.
- On the other hand, the solution may be quasi-periodic, chaotic, and even unbounded so that the previous harmonic balance Eq. (6) does not work. Note that the non-periodic solution only arises for a portion of frequencies. In this case, the frequency response data should be selected to skip this portion of frequencies so that all selected response data are periodic.

Clearly, parameter identification is realized by solving the optimization problem (12). The gradient-based methods including the sensitivity approach can be used to get the solution and in doing so, the sensitivity/gradient matrix

$$\begin{aligned} \mathbf{S}(\boldsymbol{p}) = \nabla_{\boldsymbol{p}}\boldsymbol{R}(\boldsymbol{p}) &:= \begin{bmatrix} \frac{\partial \boldsymbol{R}(\boldsymbol{p})}{\partial p_1} & \frac{\partial \boldsymbol{R}(\boldsymbol{p})}{\partial p_2} & \cdots & \frac{\partial \boldsymbol{R}(\boldsymbol{p})}{\partial p_n} \end{bmatrix} \\ &= \begin{bmatrix} \mathbf{L}\frac{\partial z(\omega_1, \boldsymbol{f}_1, \boldsymbol{p})}{\partial p_1} & \mathbf{L}\frac{\partial z(\omega_1, \boldsymbol{f}_1, \boldsymbol{p})}{\partial p_2} & \cdots & \mathbf{L}\frac{\partial z(\omega_1, \boldsymbol{f}_1, \boldsymbol{p})}{\partial p_l} \\ \mathbf{L}\frac{\partial z(\omega_2, \boldsymbol{f}_2, \boldsymbol{p})}{\partial p_1} & \mathbf{L}\frac{\partial z(\omega_2, \boldsymbol{f}_2, \boldsymbol{p})}{\partial p_2} & \cdots & \mathbf{L}\frac{\partial z(\omega_2, \boldsymbol{f}_2, \boldsymbol{p})}{\partial p_l} \\ \vdots & \vdots & \ddots & \vdots \\ \mathbf{L}\frac{\partial z(\omega_l, \boldsymbol{f}_l, \boldsymbol{p})}{\partial p_1} & \mathbf{L}\frac{\partial z(\omega_l, \boldsymbol{f}_l, \boldsymbol{p})}{\partial p_2} & \cdots & \mathbf{L}\frac{\partial z(\omega_l, \boldsymbol{f}_l, \boldsymbol{p})}{\partial p_l} \end{bmatrix}. \end{aligned} \tag{13}$$

is essentially computed. To get this sensitivity matrix $\mathbf{S}(\boldsymbol{p})$, the sensitivity analysis should be conducted to compute $\frac{\partial z(\omega, \boldsymbol{f}_0, \boldsymbol{p})}{\partial p_i}, i = 1, 2, \ldots, n$, as will be elaborated in the next subsection.

3.2 Sensitivity analysis

To compute the sensitivity $\frac{\partial z(\omega, \boldsymbol{f}_0, \boldsymbol{p})}{\partial p_i}$, differentiation of Eq. (6) with respect to p_i yields

$$\mathbf{A}(\omega)\frac{\partial \boldsymbol{z}}{\partial p_i} + \frac{\partial \boldsymbol{F}_{nl}(\omega, \boldsymbol{z})}{\partial \boldsymbol{z}}\frac{\partial \boldsymbol{z}}{\partial p_i} + \frac{\partial \boldsymbol{F}_{nl}(\omega, \boldsymbol{z})}{\partial p_i} + \frac{\partial \mathbf{A}(\omega)}{\partial p_i}\boldsymbol{z} = \mathbf{0} \tag{14}$$

where the external forces $\boldsymbol{F}$ are assumed independent of $\boldsymbol{p}$, and $\frac{\partial \boldsymbol{F}_{nl}(\omega,\boldsymbol{z})}{\partial \boldsymbol{z}}$, $\frac{\partial \boldsymbol{F}_{nl}(\omega,\boldsymbol{z})}{\partial p_i}$ are of the following forms:

$$\frac{\partial \boldsymbol{F}_{nl}(\omega, \boldsymbol{z})}{\partial p_i} = \begin{bmatrix} \frac{1}{T}\int_0^{\mathrm{T}} \frac{\partial \boldsymbol{f}_{nl}(\dot{\boldsymbol{u}},\boldsymbol{u})}{\partial p_i}\mathrm{d}t \\ \frac{2}{T}\int_0^{\mathrm{T}} \cos(\omega t)\frac{\partial \boldsymbol{f}_{nl}(\dot{\boldsymbol{u}},\boldsymbol{u})}{\partial p_i}\mathrm{d}t \\ \frac{2}{T}\int_0^{\mathrm{T}} \sin(\omega t)\frac{\partial \boldsymbol{f}_{nl}(\dot{\boldsymbol{u}},\boldsymbol{u})}{\partial p_i}\mathrm{d}t \\ \cdots \\ \frac{2}{T}\int_0^{\mathrm{T}} \cos(N\omega t)\frac{\partial \boldsymbol{f}_{nl}(\dot{\boldsymbol{u}},\boldsymbol{u})}{\partial p_i}\mathrm{d}t \\ \frac{2}{T}\int_0^{\mathrm{T}} \sin(N\omega t)\frac{\partial \boldsymbol{f}_{nl}(\dot{\boldsymbol{u}},\boldsymbol{u})}{\partial p_i}\mathrm{d}t \end{bmatrix},$$

$$\frac{\partial \boldsymbol{F}_{nl}(\omega, \boldsymbol{z})}{\partial \boldsymbol{z}} = \left[\frac{\partial \boldsymbol{F}_{nl}(\omega, \boldsymbol{z})}{\partial \boldsymbol{a}_0}, \frac{\partial \boldsymbol{F}_{nl}(\omega, \boldsymbol{z})}{\partial \boldsymbol{a}_1}, \frac{\partial \boldsymbol{F}_{nl}(\omega, \boldsymbol{z})}{\partial \boldsymbol{b}_1}, \ldots, \frac{\partial \boldsymbol{F}_{nl}(\omega, \boldsymbol{z})}{\partial \boldsymbol{a}_N}, \frac{\partial \boldsymbol{F}_{nl}(\omega, \boldsymbol{z})}{\partial \boldsymbol{b}_N}\right],$$

$$\frac{\partial \boldsymbol{F}_{nl}(\omega, \boldsymbol{z})}{\partial \boldsymbol{a}_n} = \frac{2}{T}\int_0^{\mathrm{T}} \cos(n\omega t)\left[\frac{\partial \boldsymbol{f}_{nl}(\dot{\boldsymbol{u}}, \boldsymbol{u})}{\partial \boldsymbol{u}}\cos(n\omega t) - \frac{\partial \boldsymbol{f}_{nl}(\dot{\boldsymbol{u}}, \boldsymbol{u})}{\partial \dot{\boldsymbol{u}}} n\omega \sin(n\omega t)\right]\mathrm{d}t,$$

$$\frac{\partial \boldsymbol{F}_{nl}(\omega, \boldsymbol{z})}{\partial \boldsymbol{b}_n} = \frac{2}{T}\int_0^{\mathrm{T}} \sin(n\omega t)\left[\frac{\partial \boldsymbol{f}_{nl}(\dot{\boldsymbol{u}}, \boldsymbol{u})}{\partial \boldsymbol{u}}\sin(n\omega t) + \frac{\partial \boldsymbol{f}_{nl}(\dot{\boldsymbol{u}}, \boldsymbol{u})}{\partial \dot{\boldsymbol{u}}} n\omega \cos(n\omega t)\right]\mathrm{d}t$$

with $\frac{\partial \boldsymbol{f}_{nl}(\dot{\boldsymbol{u}},\boldsymbol{u})}{\partial \boldsymbol{u}} = [\frac{\partial \boldsymbol{f}_{nl}(\dot{\boldsymbol{u}},\boldsymbol{u})}{\partial u_1}, \frac{\partial \boldsymbol{f}_{nl}(\dot{\boldsymbol{u}},\boldsymbol{u})}{\partial u_2}, \ldots, \frac{\partial \boldsymbol{f}_{nl}(\dot{\boldsymbol{u}},\boldsymbol{u})}{\partial u_m}]$, $\frac{\partial \boldsymbol{f}_{nl}(\dot{\boldsymbol{u}},\boldsymbol{u})}{\partial \dot{\boldsymbol{u}}} = [\frac{\partial \boldsymbol{f}_{nl}(\dot{\boldsymbol{u}},\boldsymbol{u})}{\partial \dot{u}_1}, \frac{\partial \boldsymbol{f}_{nl}(\dot{\boldsymbol{u}},\boldsymbol{u})}{\partial \dot{u}_2}, \ldots, \frac{\partial \boldsymbol{f}_{nl}(\dot{\boldsymbol{u}},\boldsymbol{u})}{\partial \dot{u}_m}]$. The integration above can also be quickly computed through the AFT scheme [25,26].

By Eq. (14), the sensitivity analysis pertains obviously to a linear algebraic equation so that the sensitivity is directly and quickly obtained as:

$$\frac{\partial \boldsymbol{z}(\omega, \boldsymbol{f}_0, \boldsymbol{p})}{\partial p_i} = -\left[\mathbf{A}(\omega) + \frac{\partial \boldsymbol{F}_{nl}(\omega, \boldsymbol{z})}{\partial \boldsymbol{z}}\right]^{-1}\left(\frac{\partial \boldsymbol{F}_{nl}(\omega, \boldsymbol{z})}{\partial p_i} + \frac{\partial \mathbf{A}(\omega)}{\partial p_i}\boldsymbol{z}\right). \tag{15}$$

This constitutes one remarkable feature of the present approach, because in comparison, the sensitivity analysis on the time-domain Eq. (1) is still an ordinary equation and shall be solved by some numerical integration method [19]. In what follows, how to solve the parameter identification problem (12) by using the sensitivity matrix (13) is detailed.

3.3 Solution by sensitivity approach and trust-region constraint

Problem (12) is a typical nonlinear least-squares problem and shall be solved in an iterative manner, that is, given the initial parameters $\boldsymbol{p}^{(0)}$, the solution is updated successively as $\boldsymbol{p}^{(k+1)} = \boldsymbol{p}^{(k)} + \Delta\boldsymbol{p}^{(k)}$, $k = 0, 1, 2, \ldots$ until convergence. The key lies in how to get a reasonable update $\Delta\boldsymbol{p}$ quickly from the prescribed parameters $\bar{\boldsymbol{p}}$ such that $g(\bar{\boldsymbol{p}} + \Delta\boldsymbol{p})$ becomes as small as possible. A common way to cope with this nonlinear least-squares problem (12) is to linearize the residual $\hat{\boldsymbol{R}} - \boldsymbol{R}(\boldsymbol{p})$ at $\bar{\boldsymbol{p}}$ [28]

$$\hat{\boldsymbol{R}} - \boldsymbol{R}(\boldsymbol{p}) \approx \Delta\boldsymbol{R}(\bar{\boldsymbol{p}}) - \mathbf{S}(\bar{\boldsymbol{p}})\Delta\boldsymbol{p};\ \Delta\boldsymbol{R}(\bar{\boldsymbol{p}}) := \hat{\boldsymbol{R}} - \boldsymbol{R}(\bar{\boldsymbol{p}});\ \Delta\boldsymbol{p} = \boldsymbol{p} - \bar{\boldsymbol{p}} \tag{16}$$

where $\mathbf{S}(\bar{\boldsymbol{p}})$ is the sensitivity matrix, as is defined in Eq. (13) and computed in Sect. 3.2.

Substitution of Eq. (16) in Eq. (12), a linear least-squares approximation to the original nonlinear goal function $g(\boldsymbol{p})$ is obtained, that is,

$$\tilde{g}(\Delta\boldsymbol{p}, \overline{\boldsymbol{p}}) = \|\Delta\boldsymbol{R}(\overline{\boldsymbol{p}}) - \mathbf{S}(\overline{\boldsymbol{p}})\Delta\boldsymbol{p}\|_{\mathbf{W}}^2 \tag{17}$$

and then, the update $\Delta\boldsymbol{p}$ can be directly solved. However, the least-squares problem (17) is often ill-posed and therefore, the Tikhonov regularization [29] shall be utilized, yielding the following update:

$$\begin{aligned}\Delta\boldsymbol{p}_\lambda &= \arg\min_{\Delta\boldsymbol{p}} \|\Delta\boldsymbol{R}(\overline{\boldsymbol{p}}) - \mathbf{S}(\overline{\boldsymbol{p}})\Delta\boldsymbol{p}\|_{\mathbf{W}}^2 + \lambda||\Delta\boldsymbol{p}||^2 \\ &= \left(\mathbf{S}^{\mathrm{T}}(\bar{\boldsymbol{p}})\mathbf{W}\mathbf{S}(\bar{\boldsymbol{p}}) + \lambda\mathbf{I}\right)^{-1}\mathbf{S}^{\mathrm{T}}(\bar{\boldsymbol{p}})\mathbf{W}\Delta\boldsymbol{R}(\bar{\boldsymbol{p}})\end{aligned} \tag{18}$$

where $||\cdot||$ is the usual ℓ^2-norm of a vector, $\mathbf{I}$ denotes the identity matrix and $\lambda \geq 0$ is just the regularization parameter. The regularization parameter λ can be obtained by the well-known L-curve method [30,31], which has been widely and successfully applied in a number of inverse problems, e.g. damage identification [16], hysteretic parameter identification [19]. Notwithstanding, the convergence of the L-curve method is not guaranteed and may result in failure for strong nonlinear problems.

To enhance the convergence of the sensitivity approach, the trust-region constraint shall be introduced, which tries to make the simplified goal function $\tilde{g}(\Delta\boldsymbol{p}, \overline{\boldsymbol{p}})$

agree better with the original nonlinear goal function $g(\Delta \boldsymbol{p} + \bar{\boldsymbol{p}})$. To do so, an agreement indicator [17] is defined to measure how well the simplified goal function agrees with the original one, whose expression is given as follows:

$$\rho(\bar{\boldsymbol{p}}, \Delta \boldsymbol{p}) := \frac{g(\bar{\boldsymbol{p}}) - g(\bar{\boldsymbol{p}} + \Delta \boldsymbol{p})}{\tilde{g}(0, \bar{\boldsymbol{p}}) - \tilde{g}(\Delta \boldsymbol{p}, \bar{\boldsymbol{p}})} = \frac{\|\Delta \boldsymbol{R}(\bar{\boldsymbol{p}})\|_{\mathbf{W}}^2 - \|\Delta \boldsymbol{R}(\bar{\boldsymbol{p}} + \Delta \boldsymbol{p})\|_{\mathbf{W}}^2}{\|\Delta \boldsymbol{R}(\bar{\boldsymbol{p}})\|_{\mathbf{W}}^2 - \|\Delta \boldsymbol{R}(\bar{\boldsymbol{p}}) - \mathbf{S}(\bar{\boldsymbol{p}})\Delta \boldsymbol{p}\|_{\mathbf{W}}^2}. \tag{19}$$

Usually, good agreement requires the agreement indicator to satisfy the following agreement condition [17]:

$$\rho(\bar{\boldsymbol{p}}, \Delta \boldsymbol{p}) \geq \rho_{cr} \in [0.25, 075] \tag{20}$$

Since $\Delta \boldsymbol{p}$ is always chosen to verify $\tilde{g}(0, \bar{\boldsymbol{p}}) - \tilde{g}(\Delta \boldsymbol{p}, \bar{\boldsymbol{p}}) \geq 0$, the agreement condition (20) guarantees that $g(\bar{\boldsymbol{p}}) \geq g(\bar{\boldsymbol{p}} + \Delta \boldsymbol{p})$, meaning that the update $\Delta \boldsymbol{p}$ is always in the descending direction of the goal function $g(\boldsymbol{p})$. In other words, the trust-region constraint is mathematically stated as: find a reasonably small update $\Delta \boldsymbol{p}$ so that the agreement criteria (20) is met.

It seems that the Tikhonov regularization and the trust-region constraint are quite different. Luckily, the trust-region constraint can be easily tackled by the Tikhonov regularization via properly selecting a regularization parameter λ. This is attributed to the fact that under the condition $\left\|\nabla_{\boldsymbol{p}} g(\overline{\boldsymbol{p}})\right\| = 2\left\|\mathbf{S}^{\mathrm{T}}(\overline{\boldsymbol{p}})\mathbf{W}\Delta \boldsymbol{R}(\overline{\boldsymbol{p}})\right\| \neq \mathbf{0}$, there holds [17]

$$\lim_{\lambda \to +\infty} \left\|\Delta \boldsymbol{p}_\lambda\right\| = 0, \quad \lim_{\lambda \to +\infty} \rho\left(\overline{\boldsymbol{p}}, \Delta \boldsymbol{p}_\lambda\right) = 1 > \rho_{cr} \tag{21}$$

where the $\Delta \boldsymbol{p}_\lambda$ is attained through the Tikhonov regularization (refer to Eq. (18)). The equality in Eq. (21) reveals that there always exits a regularization parameter λ (large enough) to satisfy the agreement condition of the trust-region constraint (20). Inspired by this, a simple yet reliable recursive strategy [17] can be invoked to determine a proper regularization parameter λ, i.e.

1. Set the initial regularization parameter as $\lambda = \lambda_L(\bar{\boldsymbol{p}})$ via the L-curve method
2. Calculate the update $\Delta \boldsymbol{p}_\lambda$ by Eq. (18)
3. Compute the agreement indicator $\rho(\bar{\boldsymbol{p}}, \Delta \boldsymbol{p}_\lambda)$ as in Eq. (19)
4. Terminate the recursion if the agreement criteria (20) is met, otherwise, increase the regularization parameter λ up to a factor $\gamma > 1$, i.e. $\lambda = \gamma\lambda$ and then, return to step 2

Finally, by the above procedure, a reasonable regularization parameter λ as well as a proper update $\Delta \boldsymbol{p}_\lambda$ can be obtained. Following this update procedure, the eventual algorithmic details to solve problem (12) can be established, as in Algorithm 1. Noticeably, it has been proved that by considering the trust-region constraint, guaranteed weak convergence [17] is achieved, that is

$$\lim_{k \to +\infty} \left\|\nabla_{\boldsymbol{p}} g\left(\boldsymbol{p}^{(k)}\right)\right\| = 0. \tag{22}$$

Algorithm 1 Algorithmic details on frequency response sensitivity approach for nonlinear structural parameter identification

Set the initial system parameters as $\boldsymbol{p}^{(0)}$ and define the corresponding parametric space $\mathcal{A}$
Define the error tolerance of convergence criterion $tol(e.g., = 10^{-6})$ and weight matrix $\mathbf{W}$(e.g.=$\mathbf{I}$)
Fix the maximum number of iterations $N_{max}(e.g., = 100)$
Load the measured response data $\hat{\boldsymbol{R}}$, determine the harmonic order N and the selection matrix $\mathbf{L}$
Fix the maximum number of steps for trust-region procedure $N_{tr}(e.g., = 20)$
Fix the trust region parameters: the critical agreement indicator $\rho_{cr} \in [0.25, 0.75]$ (e.g., $= 0.5$) and the amplification factor $\gamma > 1$ (e.g., $= 2$)
for $k = 0 : N_{max}$ **do**
  Solve Eq. (6) to get response $\boldsymbol{R}(\boldsymbol{p}^{(k)})$
  Compute the response residual $\Delta \boldsymbol{R} := \hat{\boldsymbol{R}} - \boldsymbol{R}(\boldsymbol{p}^{(k)})$
  Do sensitivity analysis to get the sensitivity matrix $\mathbf{S}(\boldsymbol{p}^{(k)})$
  Use the L-curve method to get the regularization parameter $\lambda_L\left(\boldsymbol{p}^{(k)}\right)$
  for $i = 1 : N_{tr}$ **do**
    $\lambda = \gamma^{i-1}\lambda_L\left(\boldsymbol{p}^{(k)}\right)$
    Compute the update $\Delta \boldsymbol{p} = \left(\mathbf{S}^{\mathrm{T}}(\boldsymbol{p}^{(k)})\mathbf{W}\mathbf{S}(\boldsymbol{p}^{(k)}) + \lambda \boldsymbol{I}\right)^{-1}\mathbf{S}^{\mathrm{T}}(\boldsymbol{p}^{(k)})\mathbf{W}\Delta \boldsymbol{R}$
    if $\boldsymbol{p}^{(k)} + \Delta \boldsymbol{p} \notin \mathcal{A}$ **then**
      continue
    end if
    Solve Eq. (6) to get response $\boldsymbol{R}\left(\boldsymbol{p}^{(k)} + \Delta \boldsymbol{p}\right)$
    Compute the new response residual $\Delta \boldsymbol{R}_{new} := \hat{\boldsymbol{R}} - \boldsymbol{R}(\boldsymbol{p}^{(k)} + \Delta \boldsymbol{p})$
    Calculate agreement indicator $\rho = \frac{\|\Delta \boldsymbol{R}(\boldsymbol{p}^{(k)})\|_{\mathbf{W}}^2 - \|\Delta \boldsymbol{R}_{new}\|_{\mathbf{W}}^2}{\|\Delta \boldsymbol{R}(\boldsymbol{p}^{(k)})\|_{\mathbf{W}}^2 - \|\Delta \boldsymbol{R}(\boldsymbol{p}^{(k)}) - \mathbf{S}(\boldsymbol{p}^{(k)})\Delta \boldsymbol{p}\|_{\mathbf{W}}^2}$
    if $\rho \geq \rho_{cr}$ **then**
      break
    end if
  end for
  Update the parameters $\boldsymbol{p}^{(k+1)} = \boldsymbol{p}^{(k)} + \Delta \boldsymbol{p}$
  if $\|\Delta \boldsymbol{p}\| / \left\|\boldsymbol{p}^{(k+1)}\right\| \leq tol$ **then**
    break
  end if
end for

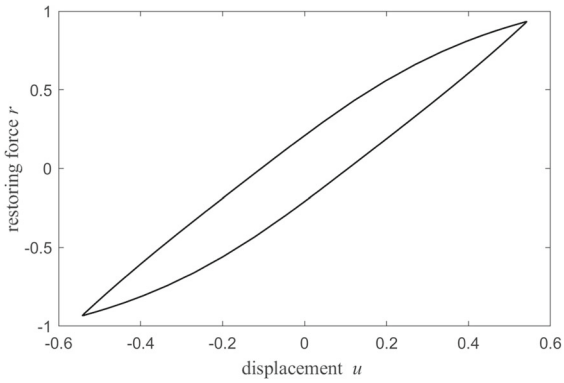

Fig. 1 Restoring force of Bouc–Wen system

4 Numerical examples

In this section, three numerical examples concerning a non-smooth single-degree-of-freedom (SDOF) hysteretic system, a five-storey structure with cubic nonlinearity and a continuous beam with geometrical nonlinearity are studied to testify the effectiveness and efficiency of the proposed approach. In practice, the transducers are often placed on the structure to get the time response data, e.g. displacement, velocity or acceleration responses. Under this circumstance, the frequency response data, i.e. $\hat{\boldsymbol{a}}_n$ and $\hat{\boldsymbol{b}}_n$, can be quickly obtained by Fourier transformation of the acquired steady-state time response data $\hat{\boldsymbol{d}}(t)$, i.e.

$$\begin{cases} \hat{\boldsymbol{a}}_0 = \Re\mathscr{F}[\hat{\boldsymbol{d}}(t)](0), \\ \hat{\boldsymbol{a}}_n = 2\Re\mathscr{F}[\hat{\boldsymbol{d}}(t)](n\omega), n = 1, 2, \ldots, N \\ \hat{\boldsymbol{b}}_n = -2\Im\mathscr{F}[\hat{\boldsymbol{d}}(t)](n\omega), n = 1, 2, \ldots, N \end{cases} \tag{23}$$

where $\mathscr{F}[f(t)](k\omega) = \frac{1}{T}\int_0^{\mathrm{T}} f(t)\mathrm{e}^{-\mathrm{i}k\omega t}$ and $\Re, \Im$ denote the real and imaginary parts of a complex vector. Here in the numerical examples, the time displacement response $\hat{\boldsymbol{d}}$ is obtained as the simulated data by solving Eq. (1) through the Runge–Kutta method, along with the addition of the root mean squares (RMS) noise in the following form:

$$\hat{\boldsymbol{d}}(t) = \boldsymbol{d}_s(t) + e_{\text{noise}} \cdot RMS(\boldsymbol{d}_s) \cdot \boldsymbol{r}_{\text{and}} \tag{24}$$

where $\boldsymbol{d}_s(t)$ is the simulated steady-state response by numerical integration, e_{noise} denotes the noise level. $RMS(\boldsymbol{d}_s(t))$ is the RMS of the time history $\boldsymbol{d}_s(t)$, while $\boldsymbol{r}_{\text{and}}$ is a random vector pertaining to standard normal distribution. Then, by Eq. (23), the noised frequency response data are acquired.

To see the robustness and accuracy of the approach under measurement noise, Monte Carlo simulation is called in some noise cases to get 100 sets of measured data, and thereafter, 100 sets of identified results can be obtained by the proposed approach. Then, the means and standard deviations of the 100 sets of identified results can be computed, from which the standard deviations indicates the robustness, while the means along with the standard deviations reflect the accuracy.

4.1 An SDOF hysteretic system

Consider an SDOF Bouc–Wen hysteretic system, whose governing equation is given as follows:

$$\begin{cases} m\ddot{u} + c\dot{u} + ku + r = f(t), \\ \dot{r} = A\dot{u} - \beta r|r|^{n-1}|\dot{u}| - \gamma|r|^n\dot{u}. \end{cases} \tag{25}$$

Herein, the known system parameters are fixed at $m = 1$, $c = 0.2$, $k = 1$, while the hysteretic model parameters to be identified are $\boldsymbol{p} = [A, \beta, \gamma, n] = [2.0, 1.0, 0.5, 2.0]$. Assume that the excitation is $f(t) = f_0\cos(\omega t)$, and the response data are obtained with the force amplitude f_0 sweeping from 1.0 to 1.9 by the increment of 0.1 over different frequency ranges with increasing frequency of resolution 0.1.

The steady-state hysteresis loop for $\omega = 1$, $f_0 = 1$ is displayed in Fig. 1, while the steady-state displacement responses without and with noise are depicted in Fig. 2. The frequency response data at this frequency and amplitude are directly extracted from the Fourier transformation of the data, and according to results in Fig. 2, the harmonic order for HBM computation is reasonably set to $N = 7$ because higher-order (> 7) harmonics with amplitude less than 10^{-4} become negligible. To get an impression on the frequency response data, the first-order Fourier coefficients a_1, b_1 (see Eq. (2)) under the force amplitude $f_0 = 1$ with the excitation frequency sweeping increasingly from 0.6 to 3.6 are displayed in Fig. 3.

Eight cases concerning different initial parameters $\boldsymbol{p}^{(0)}$, different types, frequency ranges of the measured data and different force amplitudes, as detailed in Table 1, are considered. Particularly, in case 6, the time response data along with the time response sensitivity approach [19] for parameter identification are additionally invoked for comparison. The time response data are acquired over the time interval of 0–8s at the sampling rate of 100 Hz. To further investigate the effect of

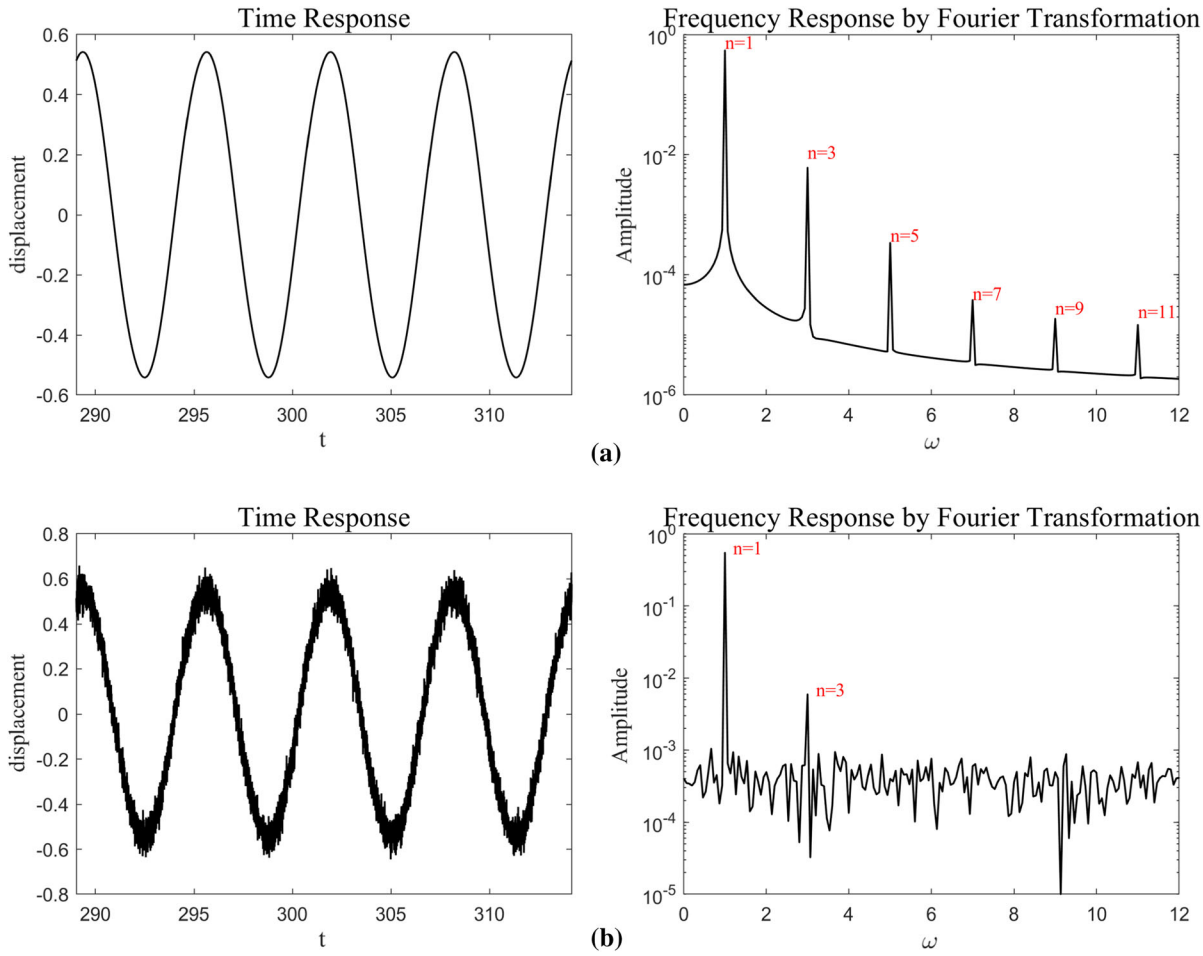

Fig. 2 Time and frequency response: **a** no noise and **b** 10% noise

Table 1 Eight identification cases for SDOF hysteretic system

Case	Initial value	Measured data	Frequency range (rad/s)	Noise level (%)
1	$\boldsymbol{p}_1^{(0)}$	a_1, b_1	[2, 2.9]	10
2	$\boldsymbol{p}_2^{(0)}$	a_1, b_1	[2, 2.9]	10
3	$\boldsymbol{p}_1^{(0)}$	b_1	[2, 2.9]	10
4	$\boldsymbol{p}_1^{(0)}$	a_1, b_1	[1, 1.9]	10
5	$\boldsymbol{p}_1^{(0)}$	a_1, b_1	[1.5, 2.4]	10
6	$\boldsymbol{p}_1^{(0)}$	$u(t)$	–	10
7	$\boldsymbol{p}_1^{(0)}$	a_1, b_1	[1.5, 3.5]	10
8	$\boldsymbol{p}_1^{(0)}$	a_1, b_1	[1.5, 3.5]	10

$\boldsymbol{p}_1^{(0)} = [1.5, 1.5, 1.5, 1.5]$
$\boldsymbol{p}_2^{(0)} = [3.0, 2.0, 2.0, 3.0]$

Table 2 Identified results of the eight cases for SDOF hysteretic system

Case	Identified results	MRE (%)	Iter#
1	2.0017, 1.0038, 0.4986, 2.0126	0.63	19
2	2.0032, 1.0017, 0.5037, 2.0120	0.74	21
3	2.0109, 0.9978, 0.5092, 1.9700	1.84	21
4	1.9932, 1.0058, 0.4839, 2.0368	3.22	30
5	2.0077, 0.9953, 0.5148, 1.9851	2.96	18
6	2.0106, 0.9911, 0.5273, 1.9951	5.46	18
7	1.9962, 1.0365, 0.4804, 2.0763	3.92	22
8	2.0036, 1.0008, 0.5034, 2.0113	0.67	18

Iter# represents the number of iterations

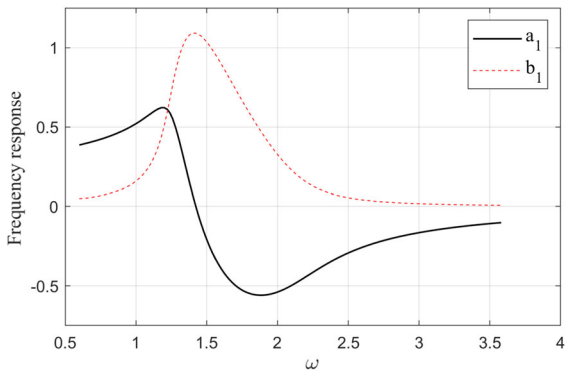

Fig. 3 Frequency response data (first order with noise level 10%) for SDOF hysteretic system

external force amplitude on the identified results, the force amplitudes are fixed to small $f_0 = 0.5$ and large $f_0 = 2$ in case 7 and case 8, respectively. By proceeding Algorithm 1, the identified results are obtained and listed in Table 2, and the relative errors are counted in Fig. 4. Here in Table 2, the maximum relative error (MRE) is defined as:

$$\text{MRE} = \max_k \left\{ \frac{|p_k - p_k^{id}|}{|p_k|} \times 100\% \right\}$$

where p_k, p_k^{id} are the respective exact and identified system parameters. All results of the eight cases show that

- In case 1 and case 2, the effect of different initial parameters is studied where the initial parameters in case 2 stay more away from the exact parameters than in case 1. As displayed in Table 2 and Fig. 4, nearly the same good identification results are obtained for both cases, indicating that the proposed approach is to some extent not sensitive to the initial parameters.
- In case 3, less data are used than in case 1. As a result, the MRE being 1.84% for case 3 is greater than 0.63% for case 1. Nevertheless, using only b_1 as the frequency data still leads to satisfactory parameter identification.
- Comparing case 4 and case 5 with case 1, the frequency data from different frequency ranges (refer to Fig. 3) are used for parameter identification. The MREs are 3.22% for case 4 and 2.96% for case 5, meaning that the parameters are all well identification. However, the errors in case 4 and case 5 are greater than that in case 1. This is reasonable because it has been shown in some publication [32] that at the resonance frequency (about ω=1.4 for this example from Fig. 3), the identification is more sensitive to noise. It is also noteworthy that if the frequency is quite away from the resonance frequency, the frequency response amplitude becomes very small. Thus, the excitation frequencies shall be selected to avoid resonance frequency, but meanwhile not far away from the resonance frequency.
- In case 6, the time response sensitivity approach [19] is adopted for parameter identification. In terms of the results in Table 2, the time response sensitivity approach also gives satisfactory parameter identification with MRE being 5.46%, though being worse than the results by the proposed approach in case 1. To further see the robustness to measurement noise of the two approaches, the Monte Carlo simulation is called where the results on the means and deviations are exhibited in Fig. 5. Clearly, the standard deviations by the proposed

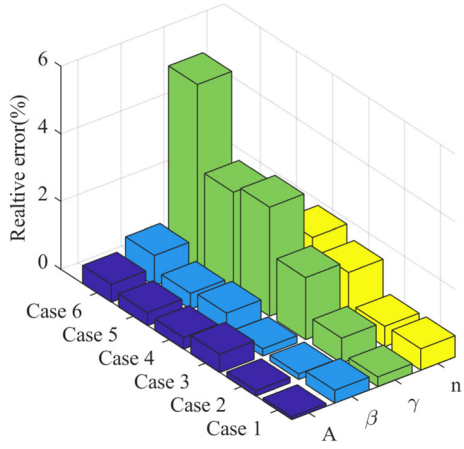

Fig. 4 Identified results for SDOF hysteretic system

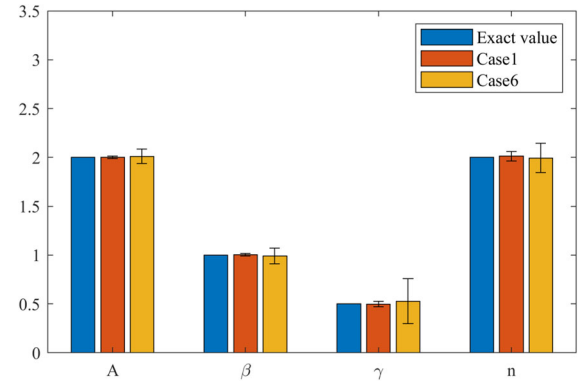

Fig. 5 Means and standard deviations of identified results by Monte Carlo simulation for SDOF hysteretic system

approach are much less than those by the time response sensitivity approach, indicating that the proposed approach is more accurate and robust.

- In case 7 and case 8, the MREs are both less than 4%, indicating that satisfactory identification is reached for both small and large force amplitudes. More specifically, the results of the large amplitude case 8 are evidently better than those of the small amplitude case 7 and this is reasonable because under a larger force amplitude, the nonlinearity is better activated and therefore, the response is more sensitive to nonlinear parameters.
- It is noteworthy from Table 2 that the number of iterations for the eight cases is no more than 30, indicating a quick convergence is achieved by the proposed approach. To visualize the convergence procedure of the proposed approach, the identified results evolving with the iterations for case 1 and case 2 are depicted in Fig. 6.

4.2 A five-storey structure

A five-storey structure with cubic nonlinear stiffness (see Fig. 7) under the sinusoidal excitation is considered in this example. The model errors are additionally taken into account. The model information for the motion equation in Eq. (1) is given as follows:

- The mass and stiffness matrices are

$$\mathbf{M} = \begin{bmatrix} m_1 & 0 & 0 & 0 & 0 \\ 0 & m_2 & 0 & 0 & 0 \\ 0 & 0 & m_3 & 0 & 0 \\ 0 & 0 & 0 & m_4 & 0 \\ 0 & 0 & 0 & 0 & m_5 \end{bmatrix},$$

$$\mathbf{K} = \begin{bmatrix} k_1+k_2 & -k_2 & 0 & 0 & 0 \\ -k_2 & k_2+k_3 & -k_3 & 0 & 0 \\ 0 & -k_3 & k_3+k_4 & -k_4 & 0 \\ 0 & 0 & -k_4 & k_4+k_5 & -k_5 \\ 0 & 0 & 0 & -k_5 & k_5 \end{bmatrix}$$

- The Rayleigh damping assumption is adopted with $\mathbf{C} = \alpha_0\mathbf{M} + \alpha_1\mathbf{K}$.
- The nonlinear restoring forces are

$$\boldsymbol{f_{nl}} = \begin{bmatrix} k_{13}{u_1}^3 - k_{23}(u_2-u_1)^3 \\ k_{23}(u_2-u_1)^3 \\ 0 \\ 0 \\ 0 \end{bmatrix}.$$

- For this structure, the parameters $m_1 = m_2 = m_3 = m_4 = m_5 = 1$, $k_3 = k_4 = k_5 = 1$ are set to be known and fixed, while other parameters including two Rayleigh damping factors α_0, α_1, linear stiffness of the first and second storey k_1, k_2 and nonlinear stiffness parameters k_{13}, k_{23} are assumed unknown and to be identified, i.e. $\boldsymbol{p} = [k_1, k_2, \alpha_0, \alpha_1, k_{13}, k_{23}]^{\mathrm{T}}$.
- An excitation force $F_1(t) = f_0 \sin(\omega t)$ is enforced on the first storey so that the external force vector is $\boldsymbol{f}(t) = [F_1(t), 0, 0, 0, 0]^{\mathrm{T}}$. Herein, to generate the frequency response data, the force amplitude f_0 sweeps from 0.5 to 1.4 by the increment of 0.1

Table 3 Identification cases of the five-storey structure

Case	Initial value	Measured data	Noise level (%)	Model error
1	$\boldsymbol{p}^{(0)}$	a_{11}	10	–
2	$\boldsymbol{p}^{(0)}$	$u_1(t)$	10	–
3	$\boldsymbol{p}^{(0)}$	a_{11}	10	$k_3, k_4, k_5(+3\%)$
4	$\boldsymbol{p}^{(0)}$	$u_1(t)$	10	$k_3, k_4, k_5(+3\%)$

$\boldsymbol{p}^{(0)} = [1.0, 1.0, 1.0, 1.0, 1.0, 1.0]$

Table 4 Identified results of the five-storey structure with weak nonlinearity

Case	Identified results	MRE (%)	Iter#
1	0.9503, 0.7995, 0.1999, 0.2502, 0.2990, 0.1506	0.37	21
2	0.9482, 0.7969, 0.1976, 0.2531, 0.3059, 0.1543	2.86	24
3	0.9540, 0.7925, 0.1856, 0.2597, 0.3158, 0.1473	7.18	21
4	0.9608, 0.7692, 0.1672, 0.2796, 0.3191, 0.1707	16.42	22

Iter# represents the number of iteration

Table 5 Identified results of the five-storey structure with strong nonlinearity

Case	Identified results	MRE (%)	Iter#
1	0.9506, 0.7997, 0.2003, 0.2499, 1.8964, 1.9982	1.87	23
2	0.9499, 0.7977, 0.1978, 0.2531, 1.9043, 1.9996	1.26	22
3	0.9479, 0.7992, 0.1889, 0.2569, 1.9667, 1.9483	5.57	23
4	0.9615, 0.7841, 0.1702, 0.2739, 1.9331, 1.9452	14.91	24

Iter# represents the number of iteration

and the frequency ω increases from 0.5 to 2.4 by increment 0.1.

To investigate the effectiveness of the proposed approach, two situations concerning weak and strong nonlinearity of the structure are studied.

4.2.1 Weak nonlinearity

The parameters to be identified for the five-storey structure with weak nonlinearity are set to $\boldsymbol{p} = [k_1, k_2, \alpha_0, \alpha_1, k_{13}, k_{23}]^{\mathrm{T}} = [0.95, 0.8, 0.2, 0.25, 0.3, 0.15]^{\mathrm{T}}$. The time and frequency responses of the first floor under the external excitation with $\omega = 1$, $f_0 = 1$ are shown in Fig. 8, from which the harmonic order for HBM computation is reasonably set to be $N = 4$ for this smooth system. The frequency response data for $f_0 = 1$ and different frequencies ω are schematically shown in Fig. 9.

Four cases as listed in Table 3 are considered to investigate the effect of data types and model errors. Herein, a_{11} represents the first element of the vector $\boldsymbol{a}_1$, and the model errors are invoked by increasing the known parameters k_3, k_4, k_5 to respective $1.03k_3$, $1.03k_4$, $1.03k_5$. In case 2 and case 4, the dis-

Table 6 Parameters of the beam

	Length (m)	Width (m)	Height (m)	Density (kg/m^3)
Beam	0.7	0.014	0.014	7800
Lamina	0.04	0.014	0.0005	7800

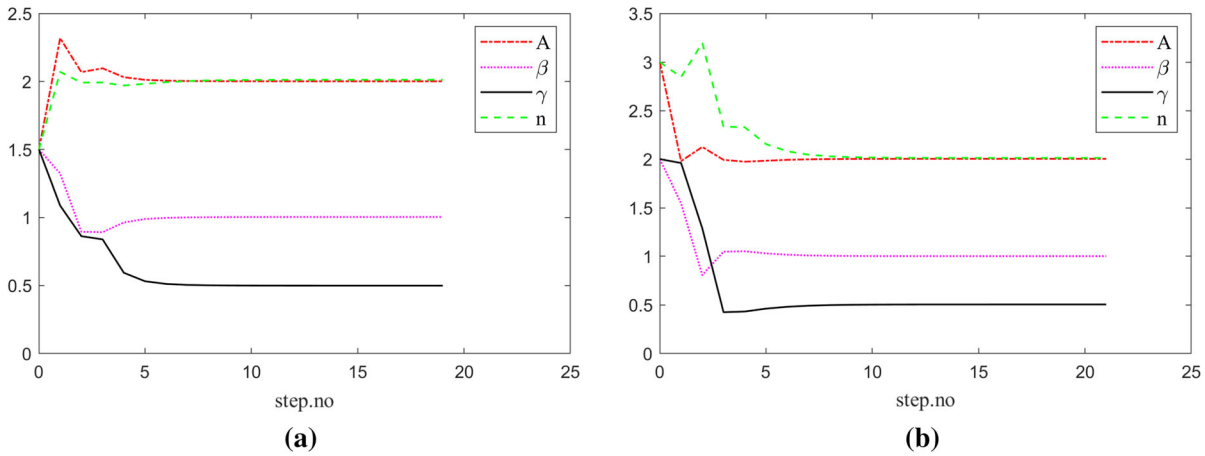

Fig. 6 Identification procedure for SDOF hysteretic system: **a** case 1 and **b** case 2

Table 7 Identification cases of the continuous beam with geometrical nonlinearity

Case	Initial value	Measured data	Noise level (%)	Grid error
1	$\boldsymbol{p}^{(0)}$	a_{A1}	10	–
2	$\boldsymbol{p}^{(0)}$	$u_A(t)$	10	–
3	$\boldsymbol{p}^{(0)}$	a_{A1}	10	Y
4	$\boldsymbol{p}^{(0)}$	$u_A(t)$	10	Y

$\boldsymbol{p}^{(0)} = [0.5, 0.5, 0.5, 0.5]$

Fig. 7 Five-storey structure

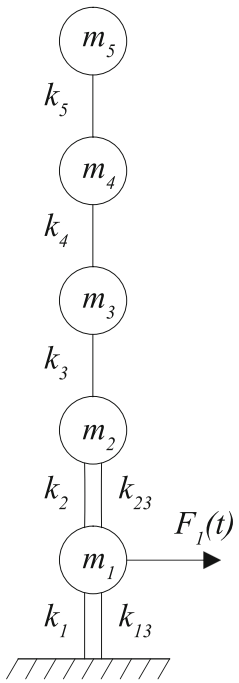

placement responses are obtained over the time interval of 0–10s at the sampling rate of 1000Hz. The proposed approach is then used for parameter identification in case 1 and case 3, while the time response sensitivity approach [19] is applied to case 2 and case 4. Identification results are summarized in Table 4, and it is observed that

- In case 1 and case 2, the MREs are respective 0.37% and 3.86%, indicating that both approaches have led to satisfactory parameter identification. Notwithstanding, the proposed approach using frequency response data is more accurate than the time response data.
- When model errors are introduced in case 3 and case 4, the MRE becomes 7.18% for case 3, while reaches 16.42% for case 4. Clearly, when model errors exist, the proposed approach still gives reasonably good identification, while parameter identification by the time response sensitivity approach is not so satisfactory. In other words, the proposed approach is found less sensitive to model errors.

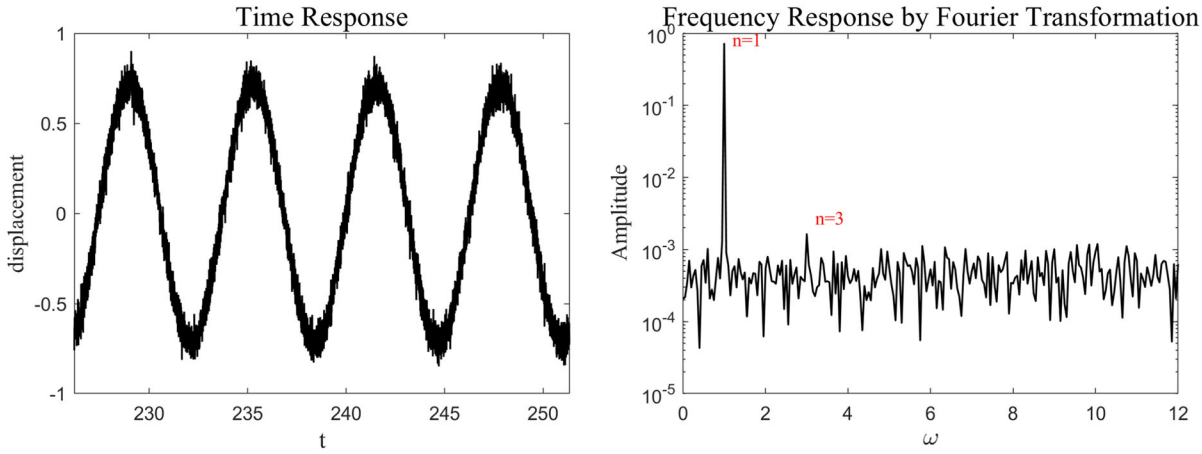

Fig. 8 Time and frequency response data under 10% noise

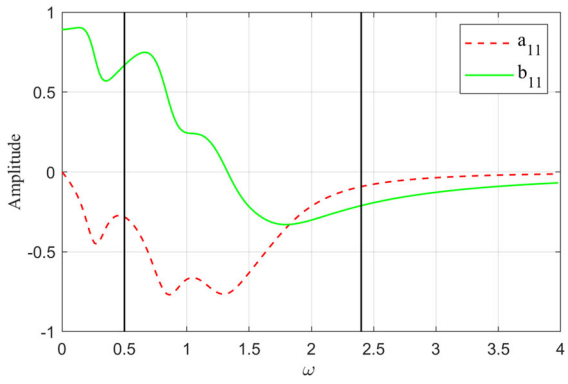

Fig. 9 Frequency response data for the five-storey structure with weak nonlinearity

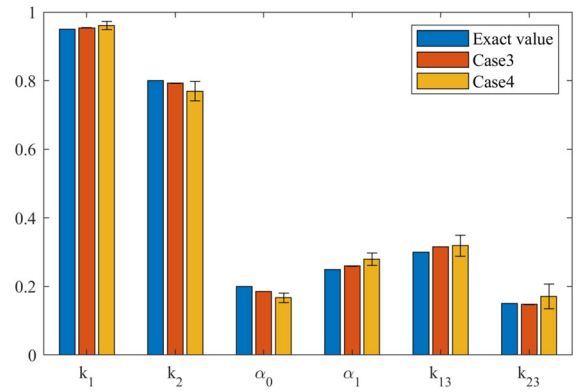

Fig. 10 Bar graph with means and standard deviations of case 3, and case 4 under weak nonlinearity

- To further see the robustness in the case of model errors, the Monte Carlo simulation is adopted for case 3 and case 4 and as a result, the means and standard deviations of the identified parameters are shown in Fig. 10. Obviously, the means of the proposed approach better approximate the exact parameters and the standard deviations are also evidently less than those by the time response sensitivity approach. To conclude, the proposed approach is more robust even when model errors exist.
- As is shown in Table 4, the number of iterations in each case is no more than 24, implying that rapid convergence by the proposed approach is achieved.

4.2.2 Strong nonlinearity

As for the five-storey structure with strong nonlinearity, the system parameters to be estimated are $\boldsymbol{p} = [k_1, k_2, \alpha_0, \alpha_1, k_{13}, k_{23}] = [0.95, 0.8, 0.2, 0.25, 1.9, 2.0]$. The same four cases in Table 3 are taken into account, and the identification results are listed in Table 6. Monte Carlo simulation is also utilized in case 3 and case 4, and the eventual results on means and deviations are depicted in Fig. 11. Obviously, in case 1 and case 2 with no model error, both approaches have given good parameter identification, while when model errors are considered in case 3 and case 4, the identification by the proposed approach is much better than by the time response sensitivity approach because much less MRE and standard deviations are acquired by the pro-

Table 8 Identified results of the beam

Case	Identified results	MRE (%)	Iter#
1	0.7010, 0.6001, 0.8075, 0.5860	2.34	20
2	0.6970, 0.6013, 0.8062, 0.5824	2.93	10
3	0.7047, 0.5992, 0.8095, 0.5805	3.25	21
4	0.7033, 0.5981, 0.7910, 0.6276	4.59	10

Iter# represents the number of iteration

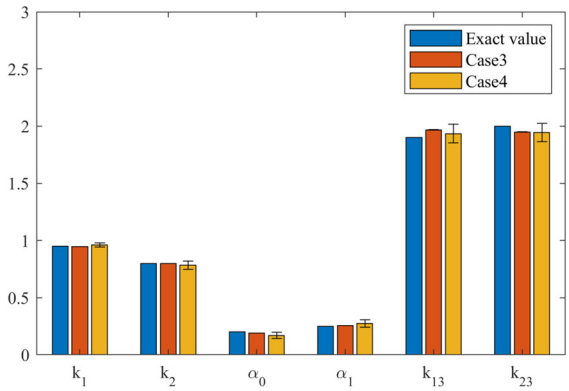

Fig. 11 Bar graph with means and standard deviations of case 3 and case 4 under strong nonlinearity

posed approach. Again, the proposed approach is found more accurate and robust for strong nonlinear parameter identification in the presence of model errors.

4.3 A continuous beam with geometrical nonlinearity

Consider a continuous beam [33] with geometrical nonlinearity which is caused by the large deflection of the lamina (see Fig. 12). The known/fixed parameters regarding the material and geometric properties of the beam are listed in Table 6. The governing equation is in the form of Eq. (1) where the Rayleigh damping $\mathbf{C} = \alpha_0\mathbf{M} + \alpha_1\mathbf{K}$ is adopted. The localized nonlinearity caused by the lamina is equivalently set to

$$f_{nl} = k_3 {u_A}^3 \tag{26}$$

where k_3 is the cubic stiffness coefficient, and u_A is the displacement of position A (the end of the main beam). For this structure, the parameters to be identified are set to $\boldsymbol{p}_u = [E, k_3, \alpha_0, \alpha_1] = [2.1 \times 10^{11}\ \text{Pa}, 5.4 \times 10^9\ \text{N/m}^3, 80\ \text{s}^{-1}, 6 \times 10^{-4}\ \text{s}]$, where E is the Young modulus. Owing to the great difference among the magnitude orders of these parameters, a simple normalization strategy $p_{uk} = p_{0k}\, p_k$ is used where $\boldsymbol{p}_0 = [p_{01}, p_{02}, p_{03}, p_{04}] = [3 \times 10^{11}\ \text{Pa}, 9 \times 10^9\ \text{N/m}^3, 100\ \text{s}^{-1}, 10^{-3}\ \text{s}]$ are prescribed and the normalized or dimensionless parameters $\boldsymbol{p} = [0.7, 0.6, 0.8, 0.6]$ are eventually to be identified. Assume that the excitation is applied at position A with the form of $f(t) = f_0 \cos(\omega t)$. The response data are obtained via sweeping the amplitude from 30 to 40 N by the increment of 1 N, and the frequency increases from 100 to 110 rad/s with the resolution of 1 rad/s (where the basic frequency of the beam is about 140 rad/s). The harmonic order of HBM is set to $N = 10$, and the number of finite elements to model the beam for parameter identification is fixed at $NE = 7$.

Four cases as detailed in Table 7 are considered to investigate the influence of measurement noise, grid error (finite element discretization error) where $u_A(t)$ is the displacement response of position A and a_{A1} is the corresponding Fourier coefficient. Note that, in case 3 and case 4, the grid/model error is introduced in the way that more elements $NE = 14$ as twice of those for parameter identification are used to get the measured data. In case 2 and case 4, the time response sensitivity approach is again utilized for comparison, where the displacement response data is obtained over the time interval of 0–0.5s at the sampling rate of 1000Hz. The identification results of the four cases are listed in Table 8, and it is shown that

- in case 1 and case 3, the MREs are both less than 3.3%, indicating that the parameters are well identified by the proposed approach even when the grid error is introduced.
- Comparing case 4 (resp. case 2) with case 3 (resp. case 1), the MRE for case 4 (resp. case 2) is 4.59% (resp. 2.93%), while the MRE for case 3 (resp. case 1) is merely 3.25% (resp. 2.34%). Though all being acceptable, the proposed approach is slightly more accurate than the time response sensitivity

Fig. 12 Continuous beam

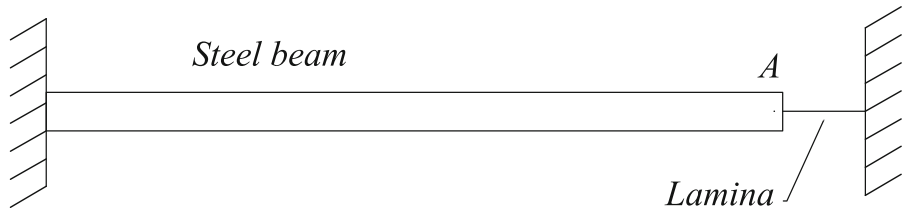

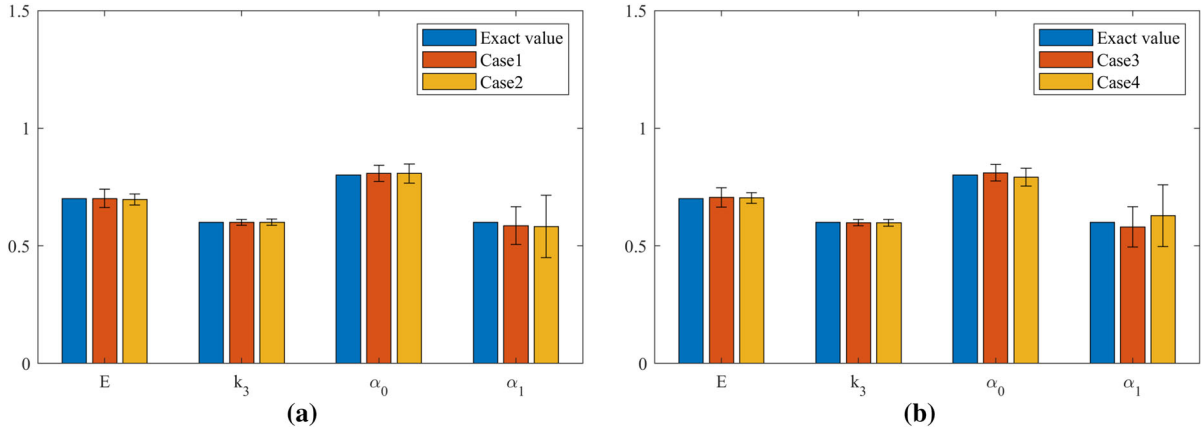

Fig. 13 Bar graph with means and standard deviations: **a** case 1 and case 2, **b** case 3 and case 4

approach. Moreover, as is displayed in Fig. 13, the standard deviation of the proposed approach is less than that of the time response sensitivity approach, implying that the proposed approach is less sensitive to the measurement noise and the grid error.

5 Conclusions

A frequency response sensitivity approach has been proposed for parameter identification of nonlinear structural systems in this paper. The attractive features are twofold. On the one hand, the frequency response data as Fourier coefficients of steady-state responses are (almost) independent from the initial conditions so that the identification will not be polluted by the inaccuracies in initial conditions. On the other hand, the frequency response data pertain to the algebraic harmonic balance equation so that the sensitivity analysis is quickly conducted by solving a linear algebraic equation. Numerical examples have been studied and results show that:

- The proposed approach is very robust to measurement noise and even under 10% noise, satisfactory parameter identification is reached. This shall be benefit from the denoise effect in acquiring the frequency response data from Fourier transformation of steady-state time responses.
- All convergence is reached within 30 iterations, indicating that rapid convergence is reached by the proposed approach.
- The proposed approach is also insensitive to model errors.
- In terms of accuracy, robustness and sensitivity to model errors, the proposed approach is found superior to the time response sensitivity approach.

Thus, the proposed approach is believed to constitute an effective and efficient tool for parameter identification of nonlinear structural systems.

Acknowledgements The present investigation was performed under the support of National Natural Science Foundation of China (Nos. 11702336 and 11972380), Guangdong Province Natural Science Foundation (No. 2018B030311001).

Declarations

Conflict of interest The authors declare that they have no conflict of interest.

References

1. Aykan, M., Özgüven, H.N.: Parametric identification of nonlinearity in structural systems using describing function inversion. Mech. Syst. Signal Process. **40**(1), 356–376 (2013)
2. Noël, J.P., Kerschen, G.: Nonlinear system identification in structural dynamics: 10 more years of progress. Mech. Syst. Signal Process. **83**, 2–35 (2017)
3. Liu, G., Wang, L., Liu, J.K., Chen, Y.M., Lu, Z.R.: Identification of an airfoil-store system with cubic nonlinear via enhanced response sensitivity approach. AIAA J. **56**(12), 4977–4987 (2018)
4. Peng, Z.K., Lang, Z.Q., Billings, S.A.: Crack detection using nonlinear output frequency response functions. J. Sound Vib. **301**(3–5), 777–788 (2007)
5. Lee, J., Fenves, G.L.: Plastic-damage model for cyclic loading of concrete structures. ASCE J. Eng. Mech. **124**(8), 892–900 (1998)
6. Li, Y., Hao, Z.: A four-parameter Iwan model and its application. Mech. Syst. Signal Process. **68–69**, 354–365 (2016)
7. Nayfeh, A.H., Mook, D.T.: Nonlinear Oscillations. Wiley, New York (2008)
8. Yang, X., Turan, A., Lei, S.: Bifurcation and nonlinear analysis of a time-delayed thermoacoustic system. Commun. Nonlinear Sci. Numer. Simul. **44**, 229–244 (2017)
9. Guckenheimer, J., Holmes, P.: Nonlinear oscillations, dynamical systems and bifurcations of vector fields. J. Appl. Mech. **51**(4), 947 (1984)
10. Cunha, J., Cogan, S., Berthod, C.: Application of genetic algorithms for the identification of elastic constants of composite materials from dynamic tests. Int. J. Numer. Methods Eng. **45**(7), 891–900 (1999)
11. Liu, G.R., Chen, S.C.: Flaw detection in sandwich plates based on time-harmonic response using genetic algorithm. Comput. Methods Appl. Mech. Eng. **190**(42), 5505–5514 (2001)
12. Yuan, L.G., Yang, Q.G.: Parameter identification and synchronization of fractional-order chaotic systems. Commun. Nonlinear Sci. Numer. Simul. **17**(1), 305–316 (2012)
13. Talatahari, S., Mohaggeg, H., Najafi, K., et al.: Solving parameter identification of nonlinear problems by artificial bee colony algorithm. Math. Probl. Eng. **2014**, 1–6 (2014)
14. Hu, W., Yu, Y., Gu, W.: Parameter estimation of fractional-order arbitrary dimensional hyperchaotic systems via a hybrid adaptive artificial bee colony algorithm with simulated annealing algorithm. Eng. Appl. Artif. Intell. **68**, 172–191 (2018)
15. Wang, C., Tang, T.: Several gradient-based iterative estimation algorithms for a class of nonlinear systems using the filtering technique. Nonlinear Dyn. **77**(3), 769–780 (2014)
16. Mottershead, J.E., Link, M., Friswell, M.I.: The sensitivity method in finite element model updating: a tutorial. Mech. Syst. Signal Process. **25**, 2275–2296 (2011)
17. Lu, Z.R., Wang, L.: An enhanced response sensitivity approach for structural damage identification: convergence and performance. Int. J. Numer. Methods Eng. **111**(13), 1231–1251 (2017)
18. Wang, L., Liu, J., Lu, Z.R.: Incremental response sensitivity approach for parameter identification of chaotic and hyperchaotic systems. Nonlinear Dyn. **89**(1), 153–167 (2017)
19. Lu, Z.R., Yao, R., Wang, L., et al.: Identification of nonlinear hysteretic parameters by enhanced response sensitivity approach. Int. J. NonLinear Mech. **96**, 1–11 (2017)
20. Lu, Z.R., Liu, G., Liu, J., et al.: Parameter identification of nonlinear fractional-order systems by enhanced response sensitivity approach. Nonlinear Dyn. **95**(2), 1495–1512 (2019)
21. Huynh, D., He, J., Tran, D.: Damage location vector: a non-destructive structural damage detection technique. Comput. Struct. **83**(28–30), 2353–2367 (2005)
22. Živanović, S., Pavic, A., Reynolds, P.: Modal testing and FE model tuning of a lively footbridge structure. Eng. Struct. **28**(6), 857–868 (2006)
23. Peng, Z.K., Lang, Z.Q., Billings, S.A.: Linear parameter estimation for multi-degree-of-freedom nonlinear systems using nonlinear output frequency-response functions. Mech. Syst. Signal Process. **21**(8), 3108–3122 (2007)
24. Peng, Z.K., Lang, Z.Q., Billings, S.A.: Nonlinear parameter estimation for multi-degree-of-freedom nonlinear systems using nonlinear output frequency-response functions. Mech. Syst. Signal Process. **22**(7), 1582–1594 (2008)
25. Krack, M., Gross, J.: Harmonic Balance for Nonlinear Vibration Problems. Springer, New York (2019)
26. Cameron, T.M., Griffin, J.H.: An alternating frequency/time domain method for calculating the steady-state response of nonlinear dynamic systems. J. Appl. Mech. **56**(1), 149–154 (1989)
27. Lu, Z.R., Zhou, J., Wang, L.: On choice and effect of weight matrix for response sensitivity-based damage identification with measurement and model errors. Mech. Syst. Signal Process. **114**, 1–24 (2019)
28. Moré, J.J.: The Levenberg–Marquardt Algorithm: Implementation and Theory. Numerical Analysis, pp. 105–116. Springer, Berlin (1978)
29. Tikhonov, A.N.: On the solution of ill-posed problems and the method of regularization. Sov. Math. **4**, 1035–1038 (1963)
30. Hansen, P.C.: Analysis of discrete ill-posed problems by means of the L-curve. SIAM Rev. **34**(4), 561–580 (1992)
31. Hansen, P.C.: Regularization tools: a Matlab package for analysis and solution of discrete ill-posed problems. Numer. Algorithms **6**(1), 1–35 (1994)
32. Guo, J., Wang, L., Takewaki, I.: Frequency response-based damage identification in frames by minimum constitutive relation error and sparse regularization. J. Sound Vib. **443**, 270–292 (2019)
33. Kerschen, G., Lenaerts, V., Golinval, J.C.: Identification of a continuous structure with a geometrical non-linearity. Part I: conditioned reverse path method. J. Sound Vib. **262**(4), 889–906 (2003)